Imaging Apoptosis with ^{99m}Tc-Annexin-V in Experimental Subacute Myocarditis

Can Peker, MD[1]; Laure Sarda-Mantel, MD[1]; Paule Loiseau[1]; François Rouzet, MD[1]; Lubna Nazneen[1]; Geneviève Martet[1]; Jean-Marc Vrigneaud, PhD[1]; Alain Meulemans, PhD[1]; Georges Saumon, MD[1]; Jean-Baptiste Michel, MD, PhD[2]; and Dominique Le Guludec, MD, PhD[1]

[1]*Équipe d'Accueil 35 12, Faculté Bichat-Claude Bernard et Service de Médecine Nucléaire de l'hôpital Bichat, Assistance Publique-Hôpitaux de Paris, Paris, France; and* [2]*Institut National de la Santé et de la Recherche Médicale, Unité 460, Unité de Formation et de Recherche Bichat, Paris, France*

^{99m}Tc-Annexin-V (ANX), which allows in vivo detection of apoptotic cells, is potentially a promising noninvasive tool to diagnose myocarditis. To test this assumption, we compared the myocardial uptake of ANX (imaging and quantitative autoradiography) in experimental subacute myocarditis (Wistar Bonn/Kobori rats [WBN/Kob]) and in normal Wistar rats. WBN/Kob is an inbred strain of Wistar rat in which myocardial injury mimicking subacute catecholamine-induced myocarditis spontaneously develops (course duration, 18 mo). The apoptotic myocardial rates were determined by immunohistochemical studies. **Methods:** Fourteen WBN/Kob rats (8–10 mo old) and 12 control rats were injected with ANX (7.4 MBq/100 g). Ten-minute anterior planar thoracic images (matrix, 128 × 128) were obtained using a pinhole collimator, 1 and 4 h after injection. Heart-to-lung activity ratios were calculated on the scintigrams. Four hours after ANX injection, quantitative autoradiography of myocardial slices was performed, as well as histologic studies with hematoxylin–eosin and with a staining assay specific for apoptotic cells. **Results:** Heart-to-lung activity ratios were higher in WBN/Kob rats than in control rats on 4-h images (2.07 ± 0.07 vs. 1.66 ± 0.06, $P = 0.0007$). Autoradiographic studies showed moderate diffuse, homogeneous myocardial ANX uptake significantly higher in WBN/Kob rats than in control rats: 54 ± 4 versus 37 ± 3 counts/mm^2 ($P < 0.007$). The apoptotic rate, evaluated with an apoptotic cell–staining assay, was 0.51% ± 0.14% of cells in WBN/Kob rats versus 0.0042% ± 0.0008% in control rats ($P < 0.008$). **Conclusion:** Compared with control rats, rats with subacute myocarditis mimicking catecholamine-induced myocarditis showed increased ANX myocardial uptake. This suggests a potential role for ANX imaging in the diagnosis of myocarditis.

Key Words: apoptosis; ^{99m}Tc-annexin-V; myocarditis

J Nucl Med 2004; 45:1081–1086

Today, much attention is paid to the diagnosis and treatment of myocarditis, since clinical and experimental arguments suggest an affiliation between inflammatory cardiac disease and dilated cardiomyopathy (*1–4*). Deleterious immune phenomena identical to those found in idiopathic dilated cardiomyopathy persist for many weeks after the virus has disappeared in myocarditis (*5*). The long-term outcome for patients with myocarditis may be as poor as for patients with idiopathic dilated cardiomyopathy (*6,7*); recent research has focused on clinical or biologic (anticardiac autoantibodies) prognostic factors (*7,8*). The diagnosis of myocarditis is particularly difficult. Clinical presentation is highly polymorphic (heart failure, chest pain sometimes mimicking myocardial infarction, arrhythmias, syncope due to auriculoventricular block), and the electrocardiographic, biologic (serum cardiac enzyme elevation), and echocardiographic data are not specific (*4*). The positive diagnosis of myocarditis is based on histologic Dallas criteria: association of inflammatory infiltration and myocyte necrosis (*9*). However, endomyocardial biopsy is invasive, induces significant cardiovascular risk, and is insensitive because of sampling error related to the patchy distribution of the disease and high interobserver variability in histologic analysis (10%–22% sensitivity according to Mason and Dec) (*10–13*). Immunohistologic techniques are more sensitive (*14*) but are still invasive and not performed in clinical practice. ^{111}In-Antimyosin antibodies, specific for cardiac myocyte necrosis, were shown to be accurate for noninvasive scintigraphic diagnosis of acute or subacute myocarditis (*14–18*) but are no longer available for clinical use. Therefore, there is a need for noninvasive tools to diagnose myocarditis.

Besides necrosis, apoptosis (programmed cell death) is also an active mechanism of cell death in several cardiac diseases, including myocarditis (*19*). Annexin-V (ANX), a 32-kDa endogenous human protein, has a highly reversible, strictly calcium-dependent, nanomolecular affinity for the membrane phosphatidylserine (*20*). With the onset of apoptosis, early after caspase-3 activation, phosphatidylserine

Received Sep. 10, 2003; revision accepted Jan. 14, 2004.

For correspondence or reprints contact: Laure Sarda-Mantel, MD, EA 3512, Service de Médecine Nucléaire, Hôpital Bichat, 46 rue Henri Huchard, 75018 Paris, France.

E-mail: sarda@bichat.inserm.fr

at the inner leaflet of the plasmic membrane is rapidly redistributed onto the cell surface. Therefore, ANX is a sensitive marker of the early to intermediate phases of apoptosis in vitro (fluorescent fluorescein isothiocyanate ANX) and in vivo (radiolabeled ^{99m}Tc-ANX) (*21*,*22*). In animal models of liver, lung, and heart transplant rejection, the presence and the degree of ^{99m}Tc-ANX uptake were shown to correlate with histology and terminal deoxynucleotidyl transferase-mediated dUTP nick-end labeling (TUNEL) staining (which detects apoptotic-related fragmentation of DNA) (*21*). ^{99m}Tc-ANX could be a reliable noninvasive tool to diagnose myocarditis (*22–24*).

To test this assumption, we compared myocardial uptake of radiolabeled ^{99m}Tc-ANX in an inbred strain of Wistar rats with subacute myocarditis (Wistar Bonn/Kobori [WBN/Kob]) and in normal Wistar rats, using scintigraphic imaging and quantitative autoradiography (*25*). Myocardial apoptotic rates were determined by immunohistologic studies.

MATERIALS AND METHODS

Animals

Male WBN/Kob rats (Japan SLC Inc.) weighing 343–427 g (mean, 367 ± 31 g) and normal male Wistar rats weighing 315–550 g (mean, 449 ± 86 g) (Janvier) were used for this study. The animals were housed and treated in accordance with institutional guidelines for animals.

WBN/Kob is an inbred strain of Wistar rat that was initially developed as a model of adenomatous changes and adenocarcinoma of the glandular stomach. Diabetes and progressive myocardial injury mimicking catecholamine-induced subacute myocarditis spontaneously develop in the male WBN/Kob rat. Histopathologically, this disease evolves from spotty areas of myocardial necrosis at the age of 3 mo to mixed inflammation and necrosis between 5 and 12 mo and then replacement fibrosis between 12 and 18 mo (*25*).

Fourteen WBN/Kob rats (5 aged 8 mo, 9 aged 10 mo) and 12 control Wistar rats underwent ^{99m}Tc-ANX scintigraphic imaging and then were killed for autoradiographic and immunohistologic studies.

^{99m}Tc-ANX Scintigraphy

Radiolabeled ^{99m}Tc-ANX was obtained by adding 370 MBq of freshly eluted ^{99m}Tc in 0.5 mL of volume to supplied sterile vials containing lyophilized 2-iminothiolane–modified ANX and stannous tartrate (Mallinckrodt). Care was taken to avoid air contact with the preparation. After incubation for 20 min at room temperature, the preparation was diluted in sterile saline, and quality control was performed using Whatman No. 1 paper chromatography (Whatman International) with butanone as the eluent and Sep-Pak (Waters Corp.) chromatography. The radiochemical purity was always >96% using the 2 techniques.

During ANX injection and scintigraphic imaging, the rats were anesthetized with 1.0% isoflurane (Abbot) in oxygen, using a small-animal anesthesia device. ANX (7.4 MBq/100 g; Mallinckrodt) was injected into the rats through the penis vein within 1 h of radiolabeling. Anterior thoracic and whole-body static images (preset time of 10 min) were obtained 1 and 4 h after injection, using a single-head γ-camera (Gammatome II; General Electric Medical Systems) equipped with a pinhole collimator. The energy window was centered at 140 keV with a window width of 20%, and the matrix was 128 × 128. Late 24-h images (preset time of 20 min) were also obtained for a subgroup of animals (5 WBN/Kob rats, 5 control rats).

On each anterior scintigram, regions of interest were drawn over the myocardial area and the lungs (Fig. 1). Mean activity (cpm) per pixel was determined for each region of interest. Heart-to-lung activity ratios (HLR) were then calculated.

Autoradiographic Studies

Autoradiographic studies were performed after completion of the 4-h imaging (9 WBN/Kob rats, 7 control rats). The animals were killed, and the hearts were frozen to −30°C and cut with a cryostat into 20-μm-thick sections perpendicular to the short axis of the ventricle. Heart sections were exposed for 22 h in a radioimager (Instant Imager; Packard Instrument Co.) for quantitative autoradiography. According to calibration studies performed as previously reported with activity standards of tissue-equivalent homogenates, 50 counts/mm^2 of ^{99m}Tc-ANX approximated 210 kBq/mg in autoradiography (*26*).

Histopathology

Heart sections were fixed in acetone (−20°C) and stained with hematoxylin–eosin. The tissue preparations were examined for degree of interstitial edema, myocyte necrosis, and infiltration of inflammatory cells.

Apoptotic Cell–Specific Staining Assay

The Apostain assay (Alexis Corp.) was used to stain apoptotic cells on myocardial sections. This method is regarded as more

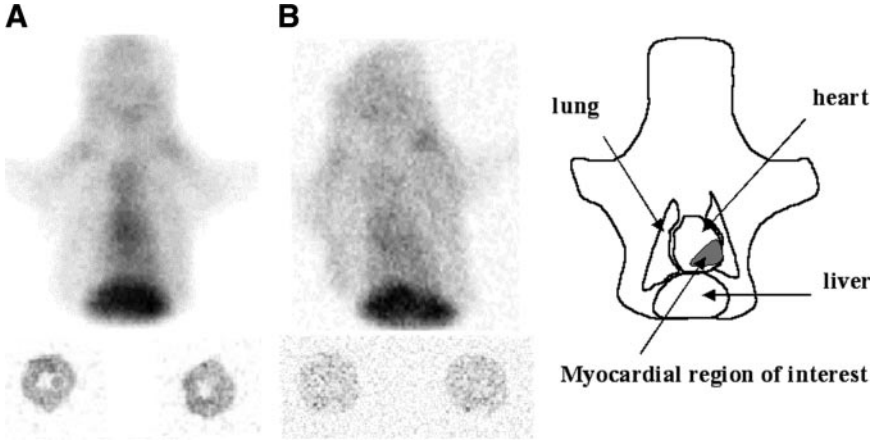

FIGURE 1. Scintigrams and autoradiographic images obtained with ANX in a WBN/Kob rat (A) and a control rat (B) 4 h after ^{99m}Tc-ANX injection. Greater tracer activity is seen in the cardiac area of the WBN/Kob rat than in the control rat on planar anterior views, corresponding to increased diffuse myocardial uptake on the autoradiogram of transaxial cardiac sections.

specific than the TUNEL method (*27*). Staining with the Apostain kit was performed according to the manufacturer's instructions. Frozen heart sections were fixed in cold 4% paraformaldehyde–phosphate-buffered saline (PBS) for 10 min, rinsed in PBS, treated with methanol:PBS (6:1) for 30 min at room temperature, and air dried. Dried sections on slides were treated in a solution of proteinase K for 20 min at room temperature and heated in formamide (56°C–60°C) for 20 min. After heating, the slides were transferred into ice-cold PBS, treated with 3% hydrogen peroxide for 5 min, blocked in 3% nonfat dry milk, and stained with monoclonal antibody F7-26 (PBS, 10 μg/mL, containing 5% fetal serum bovine) and peroxidase-conjugated antimouse IgM (1:100 in PBS). Diaminobenzidine was used as a chromogen and Hill's hematoxylin as a counterstain. The percentage of Apostain-positive cells and the number of Apostain-positive cells per square millimeter of myocardial section were estimated by light microscopy at 400-fold magnification. Any nuclei that were ambiguous were not counted. Round, homogeneous, dark dots (considered to be artifacts) and stained cell debris were carefully eliminated from counting. Brownish nucleuslike deposits, considered to be formalin crystals, were not counted. A minimum of 10,000 cells was counted for each animal.

CD4 and CD8 Immunoassay

To confirm inflammation, staining with mouse antirat cluster designation 4 (CD4) and antirat cluster designation 8 (CD8) monoclonal antibodies (BD Pharmingen) on acetone-fixed frozen heart sections was also performed, according to the manufacturer's instructions.

Statistical Analysis

Data are expressed as mean ± SEM. Groups were compared using the unpaired *t* test. The level of significance was set at $P < 0.05$.

RESULTS

On all scintigrams, nonspecific ANX activity was observed in the liver and the kidneys, in agreement with previous biodistribution studies (*20*). On the scintigrams obtained 1 h after injection, significant blood-pool activity in the cardiac cavities was observed in all animals; the HLRs were comparable in WBN/Kob and control rats: 2.59 ± 0.19 versus 2.42 ± 0.28 (not statistically significant). On the scintigrams obtained 4 h after injection, the blood-pool activity decreased, allowing visualization of cardiac ANX activity higher in WBN/Kob rats than in control rats, with HLRs significantly higher than in control rats: 2.07 ± 0.07 versus 1.66 ± 0.06 ($P = 0.0007$) (Figs. 1 and 2). Thirteen of 14 WBN/Kob rats had an HLR superior to 1.8, whereas 9 of 11 control rats had an HLR inferior to 1.8. Late, 24-h, images obtained for 5 WBN/Kob rats and 5 control rats were not interpretable because of low quality (low counting rates).

Autoradiographic studies showed diffuse, homogeneous myocardial ANX uptake significantly higher in WBN/Kob rats than in control rats: 54 ± 4 counts/mm^2 versus 37 ± 3 counts/mm^2 ($P < 0.007$) (Figs. 1 and 2).

Histopathologic analyses with hematoxylin–eosin staining in WBN/Kob rats demonstrated patchy areas of interstitial edema with inflammatory cells in the perivascular areas and at cardiocyte layers, and myocyte necrosis with nuclear extrusion, scattered throughout the myocardium (Fig. 3A). Staining with anti-CD4 and anti-CD8 monoclonal antibodies was negative in control rats and positive in WBN/Kob rats, as seen in Figure 3B. No positive staining of myocardial nuclei was observed with Apostain in control rats. Positively stained cell nuclei were found in all WBN/Kob rats and were diffusely distributed throughout the myocardium, with homogeneous or heterogeneous density (Fig. 3A). Apostain-positive cells were usually myocytes and occasionally inflammatory cells. The mean percentage of Apostain-positive cells was 0.506% ± 0.140% in WBN/Kob rats, versus 0.0042% ± 0.0008% in control rats ($P < 0.008$) (Fig. 2). The mean number of Apostain-positive cells per square millimeter of myocardial section was 16 ± 8 in WBN/Kob rats, versus 0.16 ± 0.08 in control rats ($P = 0.008$).

DISCUSSION

In this preclinical study, we observed homogeneous myocardial ANX uptake, which was greater in rats with progressive myocardial injury mimicking subacute catecholamine-induced myocarditis than in control rats, on both in vivo scintigraphic images and ex vivo heart quantitative autoradiographs.

WBN/Kob rats provide a model of hereditary catecholamine-induced myocarditis that develops progressively between 3 and 18 mo of age (*25*). At 1 mo of age, electrocardiographic abnormalities appear, including a significantly larger QRS complex amplitude, a smaller T-wave amplitude, a longer QRS duration, and a longer QT interval, as well as hypersensitivity to the chronotropic effect of iso-

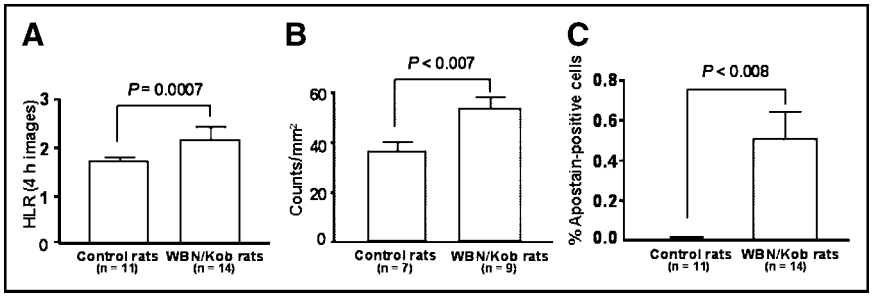

FIGURE 2. Comparative histograms of WBN/Kob and control rats: HLR on 4-h scintigrams (A), ANX uptake on myocardial autoradiograms (B), and percentage of Apostain-positive myocardial cells on 5-μm myocardial sections (C). The error bars represent SEM.

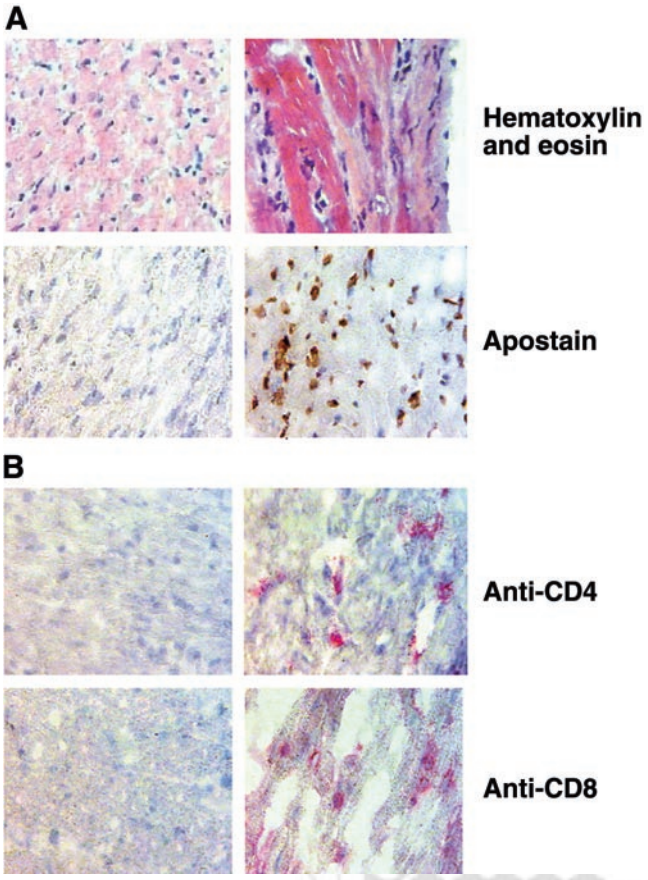

FIGURE 3. (A) Hematoxylin–eosin and Apostain staining of transverse heart sections. No positive staining is seen with Apostain in the control heart (left), whereas typical Apostain-positive brownish nuclei are observed in the heart of the WBN/Kob rat (right). (B) Negative anti-CD4 and anti-CD8 immunostaining in transverse sections of a control heart (left), and positive anti-CD4 and anti-CD8 pink immunostaining in transverse sections of the heart of a WBN/Kob rat (right).

proterenol, a potent β-adrenergic agonist (*28*). Histopathologically, spotty necrosis of cardiac myocytes appears at the age of 3 mo. After the age of 5 mo, the area of necrosis increases in association with infiltration of inflammatory cells, as we observed with hematoxylin–eosin and anti-CD4/anti-CD8 immunohistologic studies. Myocardial damage progresses very slowly. Replacement fibrosis develops at 12 mo of age. At the age of 18 mo, massive fibrosis is observed in the middle and inner layers of the ventricle (*25*).

The other available animal models of myocarditis are pharmacologic (isoproterenol) or autoimmune myocarditis in rats and coxsackievirus myocarditis in mice (*29,30*). All these models are of acute, severe, diffuse myocarditis, which is not likely to be representative of all episodes of clinical myocarditis. Most patients with acute myocarditis have a clinically inapparent course or minimal extent of myocardial injury, with only temporary electrocardiographic changes or only segmental ventricular wall motion abnormalities. Also, after the acute phase, myocarditis can evolve to a subacute active phase clinically silent until global left ventricular function is sufficiently affected to induce symptoms not distinguishable from those of dilated cardiomyopathy. Therefore, we chose the WBN/Kob model of subacute myocarditis to evaluate the sensitivity of ANX for detecting mild myocardial disease.

^{99m}Tc-ANX allows in vivo detection of phosphatidylserine translocated at the cell surface during the apoptotic process (*23*). Phosphatidylserine represents 10%–15% of the total phospholipid content of plasma cell membrane and is normally restricted to the inner leaflet of the plasma membrane lipid bilayer by an adenosine triphosphate–dependent translocase. With the onset of apoptosis, early after caspase-3 activation, phosphatidylserine is rapidly redistributed onto the cell surface. The number of ANX binding sites per cell with the onset of apoptosis increases 100- to 1,000-fold, reaching values of 3–4 million in some cell lines. Phosphatidylserine exposure on the cell surface occurs before nuclear chromatin condensation (detected by Apostain) and DNA fragmentation (detected by the TUNEL method) (*27,31*). Many previous animal studies found early detection of induced cellular apoptosis with ANX: Fas ligand–mediated hepatic apoptosis in mice; cyclophosphamide-induced bone marrow or B-cell lymphoma apoptosis in mice; heart, lung, or hepatic transplant rejection in rats; and brain and myocardial ischemia reperfusion in rats (*22,23,32–34*). Detection of cardiac myocyte apoptosis was also reported with ANX in patients with cardiac allograft rejection (*35*). In all cases, the presence and degree of ^{99m}Tc-ANX uptake correlated with histology and TUNEL staining (which detects apoptotic-related fragmentation of DNA) (*21*). Increased ANX uptake was demonstrated 2 h after coronary reperfusion (primary transluminal coronary angioplasty) in patients with acute myocardial infarction (*36*). Besides detecting apoptosis, ANX may also detect recent necrosis, because membrane disruption in necrotic cells may allow ANX to reach phosphatidylserine located at the inner leaflet (*37–39*). The potential of ANX to detect both apoptosis and recent necrosis could indeed be advantageous for the diagnosis of myocarditis, which comprises both apoptotic and necrosed myocytes (*9,19,24*).

The gold-standard method (Apostain) we used to quantify apoptosis involves a formamide-based DNA denaturation protocol combined with detection of denatured DNA by a monoclonal antibody (F7-26) against single-strand DNA (*27*). Heating of tissue sections in the presence of formamide induces selective DNA denaturation in apoptotic but not in necrotic cells. Denatured DNA in the condensed chromatin of the apoptotic nuclei is then detected with monoclonal antibody F7-26, which specifically reacts with deoxycytidine and requires for its binding single-strand DNA of at least 25–30 bases in length. For detecting apoptotic cells, this method is regarded as more specific than the TUNEL method (*27*). We found 0.506% ± 0.140% of Apostain-positive cells, mostly myocytes, in the WBN/Kob rats studied. We did not observe any Apostain staining in the necrosed myocytes with nuclear extrusion. However, the

possibility cannot be excluded that some cells undergoing necrosis—cells in which DNA single-strand ends can be seen—may be stained with Apostain (*37*). Obviously, the rate of Apostain-positive cells we obtained is on the same order of magnitude as the rates of TUNEL-positive myocardial cells previously reported for mice with coxsackievirus B3 myocarditis (0.42% ± 0.06% of myocytes), for rats with autoimmune myocarditis at the acute phase (0.53%–0.99% of myocytes and 0.61%–1.67% of lymphocytes), and for patients with myocarditis (0.61% ± 1.25%, with a maximum rate of 6.15% in severe active myocarditis) (*29*,*30*,*19*).

This apoptotic rate is rather low. It corresponds to only 16 ± 8 apoptotic cells among 3,920 ± 972 nonapoptotic cells per square millimeter of WBN/Kob rat myocardial section. In accord with such a low apoptotic rate, the difference in HLRs on 4-h imaging between WBN/Kob and control rats was low but statistically highly significant ($P = 0.0007$). Therefore, our results confirm good sensitivity for the detection of apoptosis with ANX. In the WBN/Kob model, the amount of recent necrosis is probably very low because the myocardial damage progresses very slowly.

In accord with our results, Tokita et al. (*40*) recently reported significant ^{99m}Tc-hydrazinonicotinamide-ANX uptake in the hearts of rats with acute (3 wk after immunization) autoimmune myocarditis, with uptake values slightly higher than ours (2 times the values in control rats in their study vs. 1.46 times in ours). This finding was probably related to higher rates of apoptotic cells in the myocardium, as found by a previous study (0.53%–0.99% of TUNEL-positive myocytes and 0.61%–1.67% of TUNEL-positive lymphocytes) (*29*), or to ANX uptake in recent necrosis. Conversely, no significant ANX uptake was found 7 wk after immunization, during the "subacute" phase of inflammation, probably because of the absence of significant apoptosis: According to a previous study, TUNEL staining was negative during this phase (*29*). In fact, it seems that the apoptotic rate is higher in the WBN/Kob model than in the autoimmune model during the subacute phase, possibly because of differences in the mechanisms of myocardial injury: catecholamines in WBN/Kob rats, inflammation in autoimmune myocarditis.

The study had some limitations. The WBN/Kob model may not reflect the myocardial status of patients with subacute myocarditis, about which little is known because of high diagnostic difficulties. However, with this model we could demonstrate the ability of ANX to detect a low percentage of apoptotic cells in the myocardium. This finding is encouraging with regard to potential diagnostic value in patients with acute myocarditis, who have been shown to have increased apoptosis and recent necrosis (*19*,*10*).

CONCLUSION

Compared with control rats, rats with subacute myocardial injury mimicking catecholamine-induced myocarditis show a significant increase in myocardial ^{99m}Tc-ANX uptake. This increase is in agreement with the presence of apoptotic cells on immunohistologic studies with Apostain. The sensitivity of ^{99m}Tc-ANX seems to be high, since the apoptotic rate we found in our model was low. This sensitivity suggests that ^{99m}Tc-ANX imaging has potential value as a noninvasive in vivo method for diagnosing myocarditis in humans.

REFERENCES

1. Dec GW, Palacios IF, Fallon JT, et al. Active myocarditis in the spectrum of acute dilated cardiomyopathies. *N Engl J Med.* 1983;312:885–890.
2. Sole MJ, Liu P. Viral myocarditis: a paradigm for understanding the pathogenesis and treatment of dilated cardiomyopathy. *J Am Coll Cardiol.* 1993;22:99A–105A.
3. Luppi P, Rudert WA, Zanone MM, et al. Idiopathic dilated cardiomyopathy: a superantigen-driven autoimmune disease. *Circulation.* 1998;98:777–785.
4. Liu PP, Mason JW. Advances in the understanding of myocarditis. *Circulation.* 2001;104:1076–1082.
5. Why HJ, Meany BT, Richardson PJ, et al. Clinical and prognostic significance of enteroviral RNA in the myocardium of patients with myocarditis or dilated cardiomyopathy. *Circulation.* 1994;89:2582–2589.
6. Grogan M, Redfield MM, Bailey KR, et al. Long-term outcome of patients with proven myocarditis: comparison with idiopathic dilated cardiomyopathy. *J Am Coll Cardiol.* 1995;26:80–84.
7. McCarthy RE III, Boehmer JP, Hruban RH, et al. Long-term outcome of fulminant myocarditis as compared with acute (nonfulminant) myocarditis. *N Engl J Med.* 2000;342:734–735.
8. Lauer B, Schannwell M, Kühl U, Strauer BE, Schultheiss HP. Antimyosin autoantibodies are associated with deterioration of systolic and diastolic left ventricular function in patients with chronic myocarditis. *J Am Coll Cardiol.* 2000;35:11–18.
9. Aretz HT. Myocarditis: the Dallas Criteria. *Hum Pathol.* 1987;18:619–624.
10. Billingham MB. Acute myocarditis: a diagnostic dilemma. *Br Heart J.* 1987;58:6–8.
11. Chow LH, Radio SJ, Sears TD, McManus BM. Insensitivity of right endomyocardial biopsy in the diagnosis of myocarditis. *J Am Coll Cardiol.* 1989;14:915–920.
12. Hauck AJ, Kearney DL, Edwards WD. Evaluation of post-mortem endomyocardial biopsy specimen from 38 patients with lymphocytic myocarditis: implications for role of sampling error. *Mayo Clin Proc.* 1989;64:1235–1245.
13. Mason JW, O'Connell JB, Herskowitz A, et al. A clinical trial of immunosuppressive therapy for myocarditis. *N Engl J Med.* 1995;333:269–275.
14. Kühl U, Lauer B, Souvatzoglou M, Vosberg H, Schultheiss HP. Antimyosin scintigraphy and immunohistologic analysis of endomyocardial biopsy in patients with clinically suspected myocarditis: evidence of myocardial cell damage and inflammation in the absence of histologic signs of myocarditis. *J Am Coll Cardiol.* 1998;32:1371–1376.
15. Dec GW, Palacios IF, Yasuda T, et al. Antimyosin antibody cardiac imaging: its role in the diagnosis of myocarditis. *J Am Coll Cardiol.* 1990;16:97–104.
16. Narula J, Khaw BA, Dec W, et al. Diagnostic accuracy of antimyosin scintigraphy in suspected myocarditis. *J Nucl Cardiol.* 1996;3:371–381.
17. Sarda L, Assayag P, Palazzo E, et al. Indium 111 antimyosin antibody imaging of primary involvement in systemic diseases. *Ann Rheum Dis.* 1999;58:90–95.
18. Sarda L, Colin P, Boccara, et al. Myocarditis in patients with clinical presentation of myocardial infarction and normal coronary angiograms. *J Am Coll Cardiol.* 2001;37:786–792.
19. Alter P, Jobmann M, Meyer E, Pankuweit S, Maisch B. Apoptosis in myocarditis and dilated cardiomyopathy: does enterovirus genome persistence protect from apoptosis? An endomyocardial biopsy study. *Cardiovasc Pathol.* 2001;10:229–234.
20. Ohtsuki K, Akashi K, Aoka Y, et al. Technetium-99m HYNIC-annexin V: a potential radiopharmaceutical for the in-vivo detection of apoptosis. *Eur J Nucl Med.* 1999;26:1251–1258.
21. Van Engeland M, Nieland LJW, Ramaekers FCS, Schutte B, Reutelingsperger CPM. Annexin V-affinity assay: a review on an apoptosis detection system based on phosphatidylserine exposure. *Cytometry.* 1998;31:1–9.
22. Blankenberg FG, Tait J, Ohtsuki K, Strauss HW. Apoptosis: the importance of nuclear medicine. *Nucl Med Commun.* 2000;21:241–250.

23. Blankenberg FG, Katsikis PD, Tait FG, et al. Imaging of apoptosis (programmed cell death) with Tc99m annexin V. *J Nucl Med.* 1999;40:184–191.
24. Blankenberg FG, Strauss W. Will imaging of apoptosis play a role in clinical care? A tale of mice and men. *Apoptosis.* 2001;6:117–123.
25. Tsuruta S, Sutani T, Masuda J, et al. Mechanism of cardiac involvement in the WBN/Kob rat. *J Mol Cell Cardiol.* 1997;29:247–253.
26. Petegnief Y, Petiet A, Peker MC, Bonnin F, Meulemans A, Le Guludec D. Quantitative autoradiography using a radioimager based on a multiwire proportional chamber. *Phys Med Biol.* 1998;43:3629–3638.
27. Frankfurt OS, Krishan A. Identification of apoptotic cells by formamide-induced DNA denaturation in condensed chromatin. *J Histochem Cytochem.* 2001;49: 369–378.
28. Machida K, Doi K, Kaburaki M, et al. Electrocardiographical findings of WBN/ Kob rats. *Lab Anim.* 1990;24:288–291.
29. Ishiyama S, Hiroe M, Nishikawa T, et al. The Fas/Fas ligand system is involved in the pathogenesis of autoimmune myocarditis in rats. *J Immunol.* 1998;161: 4695–4701.
30. Kyto V, Saraste A, Fohlman J, et al. Cardiomyocyte apoptosis after antiviral WIN 54954 treatment in murine coxsackievirus B3 myocarditis. *Scand Cardiovasc J.* 2002;36:187–192.
31. Gavrieli Y, Sherman Y, Ben-Sasson SA. Identification of programmed cell death in situ via specific labeling of nuclear DNA fragmentation. *J Cell Biol.* 1992; 119:493–501.
32. Blankenberg FG, Tait JF, Strauss HW. Apoptotic cell death: its implications for imaging in the next millennium. *Eur J Nucl Med.* 2000;27:359–367.
33. Ogura Y, Krams SM, Martinez OM, et al. Radiolabeled annexin V imaging: diagnosis of allograft rejection in an experimental rodent model of liver transplantation. *Radiology.* 2000;214:795–800.
34. Blankenberg FG, Naumovski L, Tait JF, et al. Imaging cyclophosphamide-induced intramedullary apoptosis in rats using ^{99m}Tc-radiolabeled annexin V. *J Nucl Med.* 2001;42:309–316.
35. Narula J, Acio ER, Narula N, et al. Annexin-V imaging for noninvasive detection of cardiac allograft rejection. *Nat Med.* 2001;7:1347–1352.
36. Hofstra L, Liem IH, Dumont EA, et al. Visualisation of cell death in vivo in patients with acute myocardial infarction. *Lancet.* 2000;15:356:209–212.
37. Willingham MC. Cytochemical methods for the detection of apoptosis. *J Histochem Cytochem.* 1999;47:1101–1109.
38. Narula J, Zaret BL. Noninvasive detection of cell death: from tracking epitaphs to counting coffins. *J Nucl Cardiol.* 2002;9:554–560.
39. Hofstra L, Thimister P, Boersma H, Heidendal G, Kemerink G. Detection of cell death in patients with subacute myocardial infarction using technetium labelled annexin-V? [abstract]. *Circulation.* 2001;104:II-695.
40. Tokita N, Hasegawa S, Maryama K, et al. ^{99m}Tc-Hynic-annexin-V imaging to evaluate inflammation and apoptosis in rats with autoimmune myocarditis. *Eur J Nucl Med.* 2003;30:232–238.

JNM The Journal of NUCLEAR MEDICINE

Imaging Apoptosis with ^{99m}Tc-Annexin-V in Experimental Subacute Myocarditis

Can Peker, Laure Sarda-Mantel, Paule Loiseau, François Rouzet, Lubna Nazneen, Geneviève Martet, Jean-Marc Vrigneaud, Alain Meulemans, Georges Saumon, Jean-Baptiste Michel and Dominique Le Guludec

J Nucl Med. 2004;45:1081-1086.

The Journal of Nuclear Medicine is published monthly.
SNMMI | Society of Nuclear Medicine and Molecular Imaging
1850 Samuel Morse Drive, Reston, VA 20190.
(Print ISSN: 0161-5505, Online ISSN: 2159-662X)

SNMMI SOCIETY OF NUCLEAR MEDICINE AND MOLECULAR IMAGING